Real-time Positioning and Tracking Technique for Endovascular Untethered Microrobots Propelled by MRI Gradients

Ouajdi Felfoul, *Member, IEEE*, Eric Aboussouan, *Member, IEEE*, Arnaud Chanu, *Member, IEEE,* and Sylvain Martel*, *Senior Member, IEEE*

***Abstract*—A real-time positioning and tracking technique for untethered devices or robots magnetically propelled by a clinical magnetic resonance imaging (MRI) system is described. The local magnetic field induced by the device, composed of a ferromagnetic material, is used as a signature to localize the device on three one-dimensional projections. A high-precision 3D circular-motion system was used to assess the precision and accuracy of this method. The integration of this technique inside propulsion and imaging MRI sequences was also achieved to demonstrate the feasibility of this tracking scheme in a closed-loop control scheme. Finally, in vivo tracking during automatic navigation of an untethered device in the carotid artery of a living animal is demonstrated.**

I. Introduction

MAGNETIC Resonance Imaging (MRI) systems are used to gather non-invasively images of the interior of the human body. MRI relies on magnetic field gradients to transform the signal coming from the body into an image. The use of MRI beyond its imaging capacity was investigated in [1]-[4] and recently, a clinical MRI system was successfully used to navigate a 1.5mm chrome steel bead into the carotid artery of a living swine [5]. The implementation of a robotic guided system based on MRI has the tremendous advantage of benefits from the hardware and software of modern scanner already installed in most hospitals.

Magnetic manipulation of devices and particles for medical applications are commonly used in research as well as in clinical practice. For example, in vivo steering of magnetic particles by an external magnet although limited to regions close to the skin while lacking feedback control is done in order to concentrate drugs in tumor regions, which is commonly known as Magnetic Drug Targeting (MDT) [6]-[13]. Although not applicable to untethered objects, magnetic fields are also used to apply a torque on a distal tip of a catheter where a permanent magnet is placed, thus helping surgeons to manipulate a surgical instrument [14].

An automated robotic system intended to operate inside the human body requires high-precision real-time positioning techniques. Most often, X-ray fluoroscopy is used to track traditional medical devices such as catheters and guide wires. Fluoroscopy is limited however to 2D plane projections and is known to have ionizing radiation with injurious effect on cells. On the other hand, optical means can be used to track microrobots where direct line of sight is possible such as the human eyes [15], but have limited or no potential applications in the remaining regions inside the human body.

We propose in this paper to use MRI to track the position of an untethered device or robot being controlled in the human blood circulatory network using magnetic gradients. We show that MRI is well suited for such application providing many advantages including but not limited to lack of radiation and enhanced tissue contrast.

II. Projection based tracking

The tracking technique described here relies on MRI that allows the acquisition of high quality images of the inside of the human body. MRI is based on the Nuclear Magnetic Resonance (NMR) phenomenon that allows the acquisition of a weighted signal generated by hydrogen protons subjected to a magnetic field. However, MRI is known to be a relatively slow imaging modality compared to CT-scan or ultrasound imaging. In fact, a high resolution MR image can take several minutes to be acquired. Even if techniques such as EPI [14] allow the acquisition of low resolution images at a rate of 10 images per second, they are unusable in a closed-loop real-time control system due to three main reasons. First, images will suffer from susceptibility artifact, due to the presence of the ferromagnetic device requiring complex algorithms to extract the position. Second, fast MR images involve the application of high gradients amplitude in order to encode the image which may induce a lot of unwanted motion on the bead by induction of displacement force on the ferromagnetic material as described in more details in [4]. Finally, the spatial resolution is generally lowered in fast imaging resulting in low quality images.

To overcome these limitations, we used projections to track the bead taking advantage of the magnetic field it

This work was supported in part by the Canada Research Chair (CRC) in Micro/Nanosystem Development, Fabrication and Validation and grants from the National Sciences and Engineering Research Council of Canada (NSERC), the Province of Québec, the Canada Foundation for Innovation (CFI) and the Fond Québecois de la Recherche sur la Nature et les Technologies (FQRNT).

S. Martel (corresponding author) is with the NanoRobotics Laboratory, Department of Computer and Software Engineering, and the Institute of Biomedical Engineering, École Polytechnique de Montréal (EPM), Montréal (Québec), P.O. Box 6079 Station Centre-ville, H3C 3A7 Canada (phone: 514 340-4711 ext. 5098; fax: 514-340-4658; e-mail: sylvain.martel@polymtl.ca).

O. Felfoul (e-mail: ouajdi.felfoul@polymtl.ca), E. Aboussouan (e-mail: eric.aboussouan@polymtl.ca), and A. Chanu (e-mail: arnaud.chanu@polymtl.ca) are with the NanoRobotics Laboratory at EPM.

induces. When subject to a strong magnetic field, a saturated ferromagnetic sphere induces a field B' (T) given by

$$\vec{B}'(P) = \frac{\mu_0}{4\pi}\left(3\frac{(\vec{m}.\vec{r})\vec{r}}{r^5} - \frac{\vec{m}}{r^3}\right) \quad (1)$$

where $\mu 0 = 4\pi.10^{-7}$ $(H.m^{-1})$is the vacuum permeability, r (m) is the distance from the center of the sphere and m $(A.m^2)$ is the magnetic moment given by:

$$\vec{m} = \frac{4}{3}\pi a^3 \vec{M}_{Sat} \quad (2)$$

where M_{Sat} (A/m) is the vector magnetization and a (m) is the radius of the sphere.

Following the application of an RF pulse, only spins precessing at frequencies within the bandwidth of the pulse will be excited. If the central frequency of the RF pulse is offset with respect to the Larmor frequency, and no external gradient is applied during the excitation, only the gradients induced by the magnetic particle will specify which spins will be excited as depicted in Fig. 1. The excited region constitutes the magnetic signature of the tracked object. We have opted for a gradient-echo implementation to meet the real-time constraint of our application even if a spin-echo sequence is more appropriate for tracking traditional medical instruments such as catheters and guide wires [16]. We have added a dephaser gradient in order to partially compensate

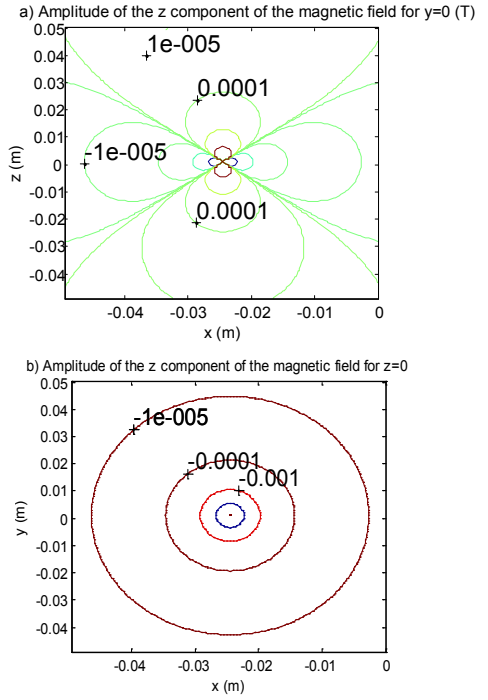

Fig. 1. Simulation of the magnetic field (T) generated from a 1mm diameter ferromagnetic bead (Bsat =1.67T) in a 1.5T surrounding field. a) Sagital or coronal cut with y =0; b) axial cut with z=0. The MRI static field is along *z*.

the phase coherence loss due to the presence of the bead induced magnetic field such as explained in [17].

I. Position Measurement

A. Relative Positioning

The relative positioning of the target can be done by simply correlating the projection P(x) with a previously acquired correlation mask M(x) as depicted in Fig. 2 [18]. Since the same magnetic element is used when M and P are acquired, they present the same distortion and thus differ only by a translation corresponding to the movement of the element between their respective acquisitions.

A computationally efficient way of performing this correlation is by doing it in the frequency domain (a.k.a. K-space):

$$C(x) = \Im^{-1}(\Im(P).*\Im(M)^*) \quad (3)$$

The position xmax of the maximum of C(x) is then used to determine the distance Δx between the mask and the current projection: Δx=xmax-L/2, with L=length(M)=length(P). Although efficient, this method has the drawback of introducing an ambiguity in the position.

B. Resolving Positional Ambiguity

Because the discrete Fourier transform assumes a periodic function, a wrap-around effect will be observed when Δx≥ L/2. The common solution to this problem would be to perform the inverse FT of M and P, pad them with L/2 zeros, perform the FT back to K-space, and then compute their correlation as seen earlier. This operation needs to be done only once for M, but has to be done again for each new P, therefore adding two FT computations to every position

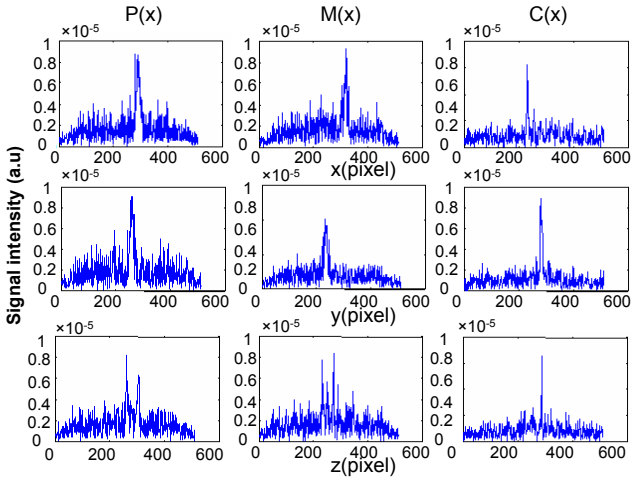

Fig. 2. (First column) Last x, y and z projections 'P(x)'; (Second column) first x, y and z projections 'M(x)' and; (Last column) their correlation 'C(x)'

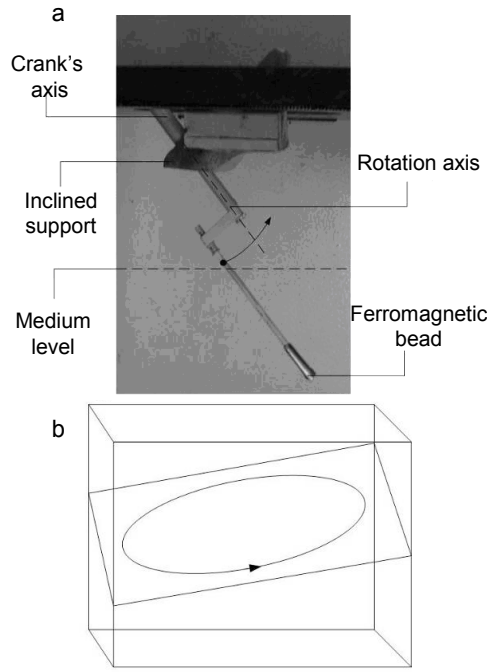

Fig. 3. (a) Photograph of the mechanical setup used to obtain a displacement along a precise 3D circle. An illustration of the circular-motion is given in (b).

evaluation. A more efficient alternative is to resolve this ambiguity heuristically, knowing that the bead or microrobot cannot leap significantly between acquisitions.

C. Absolute Positioning

The previously described method only yields relative displacements and cannot give information on the absolute position of the device with respect to the center of the MRI. This is due to the fact that the projection signal by itself doesn't have a predictable shape, since it depends on the background signal, which would allow peak finding or other simple algorithms to determine the center of the device.

By taking two readings of a position, one with positive readout gradients and one with negative readout gradients, the position of the object with regard to the center of the MRI bore can be obtained. Indeed, the shift from the center of the MRI bore will be reversed when the gradient is reversed. Convoluting the projections obtained with opposite gradients gives a maximum at a position related to the center of the device being navigated. The convolution is given by:

$$\begin{aligned} C(x) &\equiv M_{+}(x) \otimes M^{*}_{-}(x) \\ &= A(x - x_0) \otimes A^{*}(x_0 - x) \\ &= \int_{-\infty}^{\infty} A(x - x_0 - \tau) A^{*}(x_0 - \tau) d\tau \end{aligned} \quad (4)$$

where $M_{+}(x)$ is a projection mask with a magnetic element arbitrarily placed at x_0 acquired using a positive readout gradient G_R, and $M_{-}(x)$ being a mask of the same element, at the same position x_0, taken with the same readout gradient magnitude but pointing in the opposite direction ($-G_R$). $A(x-x_0)$ is the pattern describing $M_{+}(x)$. The pattern describing $M_{-}(x)$ will be a reflection of the pattern A around x_0, which is $A(x_0-x)$. The superscript * represents the complex conjugate. $C(x)$ will have its global maximum when the two A patterns overlap, that is, for $x=2*x_0$. Knowing x_0, the absolute position of the bead with respect to the center of the MRI bore; it is then possible to use the relative positioning method to get absolute positions by using M_{+} as the correlation mask. This is true because the vector (M) has been flipped as well as the pattern (A) it contains. The vectors M_{+} and M_{-} are also zero-padded to allow the computation in Fourier space without the possible wrap-around due to the implicit redundancy of the Fourier Transform (FT).

II. Positioning Resolution

A. Experimental Setup

To evaluate the 3D positioning resolution, a mechanical setup was fabricated. The setup was designed to create a specific and easily distinguishable 3D motion of the ferromagnetic bead while minimizing the motion of the surrounding medium. The setup consists on a thin, rigid pole holding a 1.5mm diameter ferromagnetic bead as depicted in Fig. 3a. The resulting motion of the pole is a precise inclined circle inducing a displacement in the three spatial axes as shown in Fig. 3b.

The experiments were conducted in a 4 liter phantom filled with water mixed with 20g/l gelatin, 1.25g/l nickel sulphate, and 5g/l NaCl, providing a semi-solid medium with shortened relaxation time for a worst case scenario. The ferromagnetic core was made of chrome-steel sphere with a diameter of 1.5mm (Salem Specialty Balls Company, Canton, CT, USA). Its magnetization at 1.5T which is the magnetic field inside the MRI system (Siemens Magnetom Avanto 1.5T, Erlangen, Germany) is $M_{1.5T} = 1.35 \times 10^6$A/m as measured with a VSM (Walker Scientific VSM, Worcester, MA, USA).

The sequence parameters used were the following: RF excitation with an offset frequency of 1.2kHz and a 30° flip angle. The time between acquisitions was 50ms leading to a refresh rate of 20 positions per second. The duration of the pulse sequence was 22.46ms and since the bead was attached to a support, no propulsion gradients were applied.

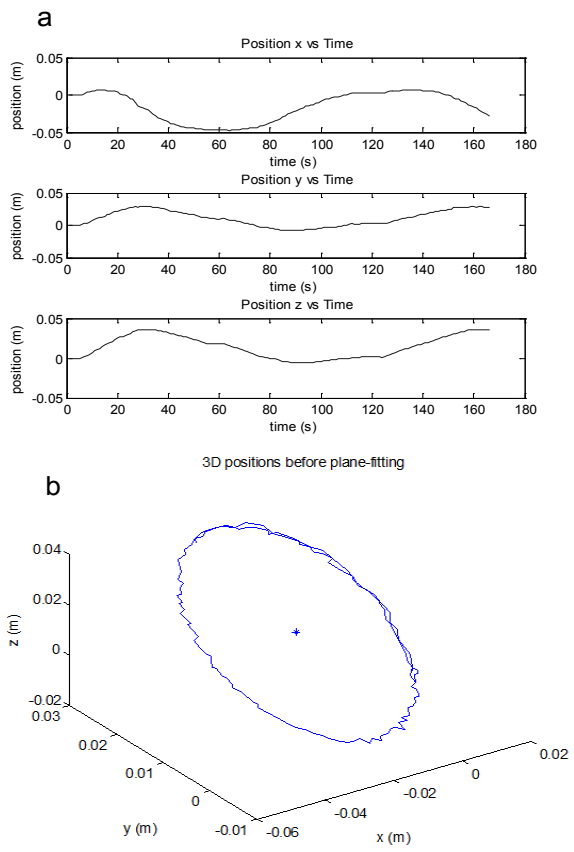

Fig. 4. (a) *x*, *y* and *z* positions versus time obtained following the sketch of the maximum of the correlation; (b) 3D graph of the positions before plane fitting,

A. Results

The positions along, *x*, *y* and *z* versus time are presented in Fig. 4a. The corresponding circle obtained with these positions before plane fitting is shown in Fig. 4b. We followed the same conventional MRI axis references where the *z* axis corresponds to the bore axis; the *y* axis is from down to top; and the *x* is from left to right. In order to accurately analyze the precision of the 3D positions obtained with this mechanical device, a first plane-fitting step was performed by Principal Component Analysis (PCA). With this change of coordinates separating the one through-plane coordinate from the two in-plane coordinates, we can find the center of rotation more precisely than using a simple center of mass as shown in Fig. 5a. The distance of the center to each position was then computed and the mean radius and standard deviation were used to assess the precision of this positioning scheme. Note that no filtering or outlier elimination techniques were used. The mean error measured was 542µm. Because of the non-negligible mechanical vibrations occurring when the setup is put in motion, this precision is considered to constitute a conservative lower bound to the real precision of the technique.

The delay between the acquisition of the *x*, *y* and *z* components also accounts for some of the discrepancies in the data. Indeed, in the right side of Fig. 5a, a slight elliptic behavior can be observed. We can also see that the points at the right are more spread than on the left side of the figure indicating that the manual operator turned the rod slightly faster in the first region. The delay between the *x* and *y* acquisitions was more significant when the bead was moving faster. This type of behavior is consistent with delay simulations in Fig. 5b when keeping in mind that the coordinates *u* and *v* of Fig. 5b have been rotated by the PCA step described earlier.

III. REAL-TIME NAVIGATION

A. Real-time Navigation Pulse Sequence

In order to be able to guide a ferromagnetic device or microrobot either inside an MR phantom or in an *in-vivo* environment, the tracking sequence must be inserted in a

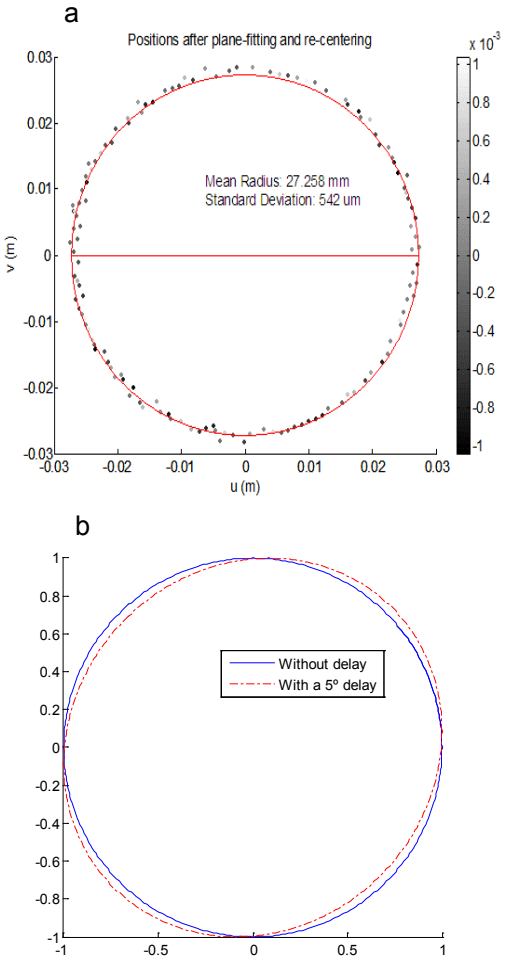

Fig. 5. (a) Positions after plane fitting and re-centering. The gray-scaled dots indicate the distance perpendicular to the plane. (b) Simulation of the delay between the *x* and *y* acquisitions.

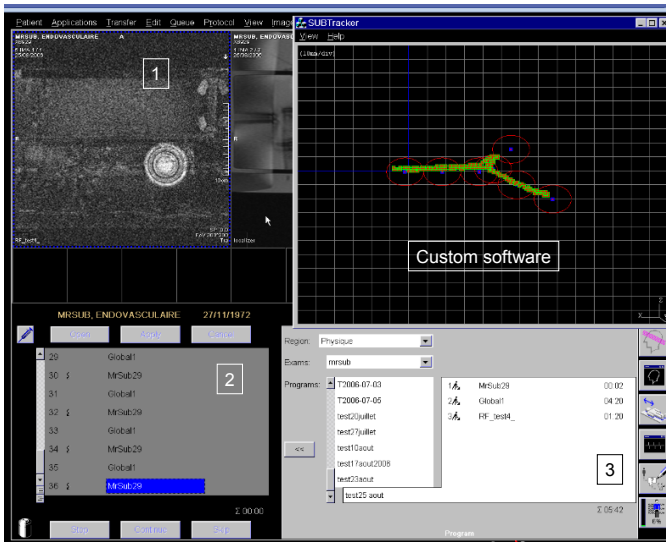

Fig. 6. User interface showing our custom software projecting the position of the bead in real-time along the pre-planned path. Numbered boxes refer to the Siemens user interface. In (1) it is shown an off-resonance image acquired to tune up the tracking sequence parameters. (2) shows the current running sequence and (3), the Siemens sequence explorer interface

real-time pulse sequence that enables real-time feedback. Fortunately, most recent clinical MRI systems allow real-time communication between the various modules [19]. Such a feedback allows the projection data to be sent to a running process located on another image data analysis computer containing the controller algorithm. Based on the obtained projection data and the expected device position, an error is computed followed by a command, namely a magnetic gradient amplitude and direction, which is sent back to the running sequence for execution. The running sequence is thus only responsible for the propulsion gradient application based on the last received computed command and for the tracking sequence execution. A real-time feedback delay must be considered for the command computation to be completed and sent back to the running sequence. This delay has been chosen to last a period of time equal to the propulsion time plus the tracking time. This feedback delay is set by the user at the beginning of the procedure. The propulsion time allowed for the bead to move is then the chosen feedback delay minus the tracking time.

B. *Path Planning*

Before the navigation procedure begins, the user executes a specific vascular image generation called an angiography. The desired path to be followed by the device is chosen during this step. Each selected position consists of waypoints, as depicted by Fig. 6, which the device under computer navigation control needs to reach before a change to the next waypoint targeted by the controller is initiated. Once the waypoint selection is completed, it is sent to the image analysis computer. During the procedure, the device's computed position is compared to the target waypoint position and a correction command is generated by the controller to be applied on the next propulsion phase.

C. *Real-time Tracking in a Phantom*

This tracking technique was successfully integrated into a propulsion sequence and a PID controller allowing real-time automatic navigational control of a microrobot in the blood vessels. A Shelley vascular phantom (Shelley Industrial Automation Inc.) placed in a container filled with water doped with a 1.25g/l of $NiSO_4.6H_2O$ was initially used for this experiment intended to assess the technique *in vitro* prior to asses it in an *in vivo* environment. The position of the sphere was visualized in real-time with custom software receiving the positions from the image calculation program and displaying them on a 2D grid as shown in Fig. 6. An overall feedback time of 41.6ms was used allowing 18.5ms for propulsion with a 24Hz tracking refresh rate.

Since the tracking technique depends on the background medium, a tuning step is required to find the best SNR [16]. This step consists on the acquisition of an image based on the same imaging timing and parameters of the tracking projections. Here, the projections that we get by running the tracking sequence are the same than the projection of the image along a given spatial axis. The optimal parameters are the ones that give a dark background and a signal coming only from the medium in the sphere's neighborhood. The parameters to be optimized are the offset frequency, the flip angle and the dephaser gradients used to recover the signal lost from magnetic field inhomogeneities.

D. *Real-time Tracking In Vivo*

In vivo experiments were performed with a 25kg domestic pig. The study was approved by the animal care and use

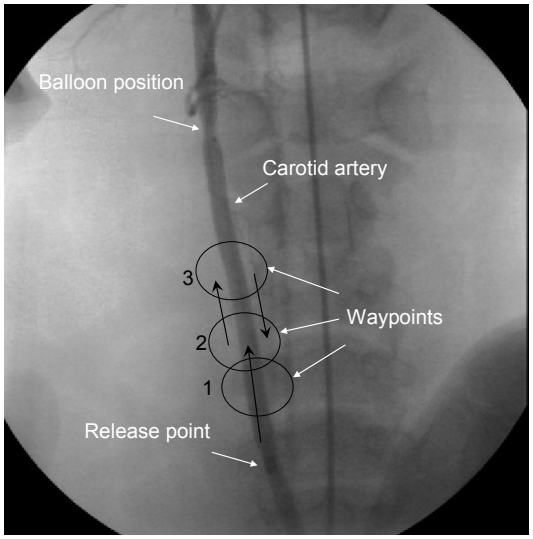

Fig. 7. X-ray image of the carotid artery of the pig. The position of the release catheter and the balloon catheter are indicated by arrows. Three waypoints were assigned to the controller. The path consists of reaching waypoints 1, 2 and 3 and performing 10 round-trips between waypoint 2 and waypoint 3.

committee of the Centre Hospitalier de l'Université de Montréal (CHUM) as well as the committee of École Polytechnique of Montréal (EPM). During the experiments, the pig was under general anesthesia.

To release the ferromagnetic bead, a 6-F, 80cm introducer catheter (Cook, Bloomington, Indiana) was used. The catheter was inserted from the left femoral artery into the carotid artery under X-ray standard interventional procedure. In addition, an angioplasty balloon (5mm×18mm angioplasty balloon - AV100, Medtronic, Santa Rosa, CA) was placed in the distal portion of the carotid artery. Its function was to control the blood flow in the carotid in order to easily retrieve the sphere. Once in the MRI interventional room, a 3D angiogram with gadoteridol injection was acquired to plan the path to be traveled. The pre-planned path consists of reaching waypoints 1, 2 and 3 and performing 10 round-trips between waypoint 2 and waypoint 3 as illustrated in Fig. 7.

IV. Conclusion

A real-time tracking technique specifically developed to locate a ferromagnetic core of an untethered microdevice or microrobot guided by magnetic gradients inside blood vessels has been described. This technique is important for the development of platforms and interventional medical micro/nanorobots operating in the human body including the cardiovascular system. This paper proved for the first time that robots with a portion made of ferromagnetic material can be positioned and tracked by an existing medical imaging modality allowing targeting and real-time closed-loop navigational control inside the human body.

Acknowledgment

We acknowledge the contribution of the Magnetic Resonance Submarine (MR-Sub) team of the NanoRobotics Laboratory and in particular, Jean-Baptiste Mathieu, Pierre Pouponneau, Samer Tamaz and Martin Mankiewicz.

References

[1] S. Martel, J. B. Mathieu, Y. L'Hocine, G. Beaudoin, and G. Soulez, "Method and system for propelling and controlling displacement of a microrobot in a blood vessel," U.S. Patent 10/417,475, Apr. 15, 2003.

[2] J. B. Mathieu, S. Martel, L'H. Yahia, G. Soulez, and G. Beaudoin, "MRI system as a mean of propulsion for a microdevice in blood vessels," in *Proc. 25th Ann. Int. Conf. IEEE-EMB*, 2003, pp. 3419-3422.

[3] S. Martel, J. B. Mathieu, O. Felfoul, H. Macicior, G. Beaudoin, G. Soulez, and Y. L'Hocine, "Adapting MRI systems to propel and guide microdevices in the human blood circulatory system," in Proc. 26th Ann. Int. Conf. IEEE-EMBS, 2004, pp. 1044-1047.

[4] J. B. Mathieu, G. Beaudoin, and S. Martel, "Method of propulsion of a ferromagnetic core in cardiovascular system through magnetic gradients generated by an MRI system," *IEEE Trans. Biomed. Eng.,* vol. 53, n. 2, pp. 292-299, Feb. 2006.

[5] S. Martel, J.-B. Mathieu, O. Felfoul, A. Chanu, E. Aboussouan, S. Tamaz, P. Pouponneau, G. Beaudoin, G. Soulez, L'H. Yahia, and M. Mankiewicz, "Automatic navigation of an untethered device in the artery of a living animal using a conventional clinical magnetic resonance imaging system", *Applied Physics Letters*, vol. 90, no. 11, March 2007.

[6] S.-I. Takeda, Terazono, Bungo; Mishima, Fumihito; Nakagami, Hironori; Nishijima, Shigehiro; Kaneda, Yasufumi, "Novel drug delivery system by surface modified magnetic nanoparticles," *Journal of Nanoscience and Nanotechnology*, vol. 6, n. 9-10, pp. 3269-3276, Sep./Oct. 2006.

[7] F. Mishima, S. Fujimoto, S. Takeda, Y. Izumi, S. Nishijima, "Development of control system for magnetically targeted drug delivery," *Journal of Magnetism and Magnetic Materials*, vol. 310, n.2, March 2007, pp. 2883-2885.

[8] F. Mishima, S. Takeda; Y. Izumi, S. Nishijima, "Three dimensional motion control system of ferromagnetic particles for magnetically targeted drug delivery systems," *IEEE Transactions on Applied Superconductivity*, vol. 16, n.2, June 2006, pp. 1539-1542.

[9] Z. G. Forbes, B. B. Yellen, K. A. Barbee, and G. Friedman, "An approach to targeted drug delivery based on uniform magnetic fields," *IEEE Transactions on Magnetics*, vol. 39, n. 5, Sept. 2003, pp. 3372-3377.

[10] E. J. Furlani, E. P. Furlani, "A model for predicting magnetic targeting of multifunctional particles in the microvasculature," *Journal of Magnetism and Magnetic Materials*, vol. 312, n. 1, May 2007, p 187-193.

[11] L. E. Udrea, J. C. N. Strachan, V. Badescu, O. Rotariu, "An in vitro study of magnetic particle targeting in small blood vessels," *Physics in Medicine and Biology*, vol. 51, n. 19, pp. 4869-4881, Oct. 2006.

[12] E. P. Furlani, K. C. Ng, "Analytical model of magnetic nanoparticle transport and capture in the microvasculature," in *Physical Review E*, v 73, n 6, June 2006, p 61919-1-10

[13] B. Gleich, N. Hellwig, H. Bridell, R. Jurgons, C. Seliger, C. Alexiou, B. Wolf, T. Weyh, "Design and evaluation of magnetic fields for nanoparticle drug targeting in cancer," in *IEEE Transactions on Nanotechnology*, vol. 6, n. 2, March 2007, p 164-70

[14] http://www.stereotaxis.com/

[15] K. B. Yesin, K. Vollmers, J. B. Nelson, "Guidance of magnetic intraocular microrobots by active defocused tracking," in *IEEE/RSJ International Conference on Intelligent Robots and Systems (IROS)*, vol. 4, pp. 3309-3314, 2004.

[16] O. Felfoul, J.B Mathieu, G. Beaudoin and S. Martel, "In Vivo MR Tracking Based on Magnetic Signature Selective Excitation", *IEEE Trans. Med. Imag*. vol. 27, no. 1, pp28-35, Jan. 2008.

[17] J-H. Seppenwoolde, M. A. Viergever, and C. J. G. Bakker, "Passive tracking exploiting local signal conservation: The white marker phenomenon," *Magnetic Resonance in Medicine*, vol. 50, no. 4, pp784-790, Oct. 2003.

[18] E. Aboussouan, and S. Martel, "High-precision absolute positioning of medical instruments in MRI systems," in Proc. 28th Ann. Int. Conf. IEEE-EMB, pp. 743-746. 2006.

[19] A. Chanu, O. Felfoul, G. Beaudoin, and S. Martel, "Adapting clinical MRI software environment for the real-time navigation of endovascular untethered ferromagnetic devices," *in Magnetic Resonance in medicine*, vol. 59, no. 6, pp1287-97, June. 2008.